Advanced Physical Research
Vol.7, No.3, 2025, pp.250-263
https://doi.org/10.62476/apr.73250

STRUCTURE AND MAGNETIC PROPERTIES OF THE NIFE FILMS ELECTRODEPOSITED IN NON-STATIONARY MODES

A. Trukhanov[1,2,*], K. Kadyrzhanov[2], D. Shlimas[2,3], R.Shakirzyanov[2], M. Zdorovets[2,3], T. Vershinina[4,5], N. Hundzilovich[6], G. Rymski[1], T. Zubar[1], A. Kotelnikova[1]

[1]Scientific-Practical Materials Research Centre of National Academy of Sciences of Belarus, 220072 Minsk, Belarus
[2]Engineering Profile Laboratory, L.N. Gumilyov Eurasian National University, 010008, Astana, Kazakhstan
[3]Laboratory of Solid State Physics, The Institute of Nuclear Physics, 050032, Almaty, Kazakhstan
[4]Joint Institute for Nuclear Research, 141980, Dubna, Russia
[5]Dubna State University, 141980, Dubna, Russia
[6]Belarusian State Technological University, 220006, Minsk, Belarus

Abstract. Ni-rich permalloy (NiFe) films were prepared using electrodeposition in different modes from sulfate electrolyte. As modes were determined regime of direct current (DC), pulse current (PC) and pulse-reverse current (RC). Correlation between technological modes of preparation, chemical composition, structural characteristics and magnetic parameters was established. Based on EDX data it was shown that Fe content in samples varied from 17.4 to 42.1 at.%, depending on deposition modes. It opens broad perspectives for chemical control of the permalloy films from one electrolyte. This is technologically convenient. Based on XRD data it was concluded that samples were single-phase. The surface morphology was analyzed using AFM. Pulse-reverse (RC) film surface are rough and have observable mostly fused grains, which significantly differs from DC and PC film surfaces, which are smooth and have no distinguishable grains. The R_q values of RC film is around 27.9 nm, while DC and PC films have R_q values of 9.6 nm and 4.1 nm, respectively. Based on DSC data all the phase transitions in investigates samples and their transition temperatures were detected and compared with bulk analogs. Temperature dependences of the magnetic susceptibility and field dependences of the specific magnetization were measured. Main magnetic parameters were established. It was demonstrated that the synthesized NiFe films have a significant magnetic anisotropy. It was demonstrated the correlation between NiFe electrodeposition modes and their magnetic properties. Obtained results open broad perspectives for modification of the standard electrodeposition processes of Ni-rich permalloy films preparation for practical applications in the field of magnetic sensors and shields for electromagnetic protection.

Keywords: NiFe films, electrodeposition, pulse-reverse regimes, magnetic properties.
Corresponding author: Scientific-Practical Materials Research Centre of National Academy of Sciences of Belarus, 220072 Minsk, Belarus, e-mail: *truhanov86@mail.ru*
Received: 12 May 2025; Revised: 24 July 2025; Accepted: 10 September 2025; Published: 16 October 2025.

1 Introduction

The electrodeposition (or electroplating) technique is a widely used for preparation of the alloy films and coatings. Electrodeposited alloy coatings are commonly used as decorative layers

(Oriňáková et al., 2006; Giurlani et al., 2018); physical, chemical, or electromagnetic protection of devices (Maniam & Paul, 2021; Lelevic & Walsh, 2019; Lisenkov et al., 2010; Papailiou et al., 2010); and electrodeposited alloy films have many applications in microelectronics (Zangari, 2015; Suzdaltsev, 2022; Deligianni, 2006). Moreover, electrodeposition is used in the synthesis of nanostructures (nanorods, nanopillars, nanolayers, and so on) nowadays Stine (2019); Inguanta et al. (2008); Sobha (2012); Nasirpouri (2017). Electrodeposition has many parameters (current density and voltage, pulse and pulse-reverse modes, electrolyte temperature, pH, and stirring) that are capable of influencing on the alloy deposits composition, crystal structure, and microstructure. In addition to composition control in mono, binary, ternary, and more complex alloys, electrodepositions provide the ability to obtain alloys with composition gradients Zubar et al. (2022); Rotkovich et al. (2023); Zubar et al. (2019) or even multilayer structures (Zubar et al., 2020; Vinnik et al., 2021; Warcholinski et al., 2017).

Electrodeposited NiFe alloys are of great importance in a wide range of applications. Ni-rich alloys ($Ni_{80}Fe_{20}$ "permalloy" and alloys with close composition) are magnetically soft materials with low coercivity and extremely high magnetic permeability (Vahdatid et al., 2018; Zhang et al., 2012; English et al., 1967; Rizal & Niraula, 2015). They are mostly known for their anisotropic and giant (in multilayer films) magnetoresistance and are used in magnetoresistive devices in hard disks (Lee et al., 2000; Vieux-Rochaz et al., 2000; Pasa & Schwarzacher, 1999). Moreover, they have such applications as electromagnetic shielding (Park et al., 2019; Kanafyev et al., 2022; Graf & Vance, 1988), magnetic field sensors (Seet et al., 2007; Hika et al., 1996), magnetic proximity effect and spin Hall effect (Mazraati et al., 2016; Ma et al., 2020; Zhu et al., 2018), and magnetoresistive random-access memory (MRAM) (**?**Almeida et al., 2022).

Modification of the synthesis conditions of the electrodeposited NiFe alloy structures makes it possible to obtain the widest range of their chemical composition, crystal structure and grain structure (Llavona et al., 2013). Electrodeposition bath composition, pH, bath temperature and agitation conditions, current parameters and modes, deposition in the magnetic field or ultrasonic radiation are the most common levers used to modify NiFe alloy deposits characteristics (Zubar et al., 2019; Horkans, 1981; Fedkin et al., 2023). Thus, pulsed electrodeposition allows to change NiFe alloys features significantly as compared to the alloys electrodeposited in direct current (Zubar et al., 2021; Salem et al., 2012; Grimmett et al., 1993). Pulse current duration and pause combination expand Fe content range (upside mostly) and decrease crystallites and grain sizes in particular (Kockar et al., 2004; Torabinejad et al., 2017; Blythe et al., 1996).

Pulse-reverse electrodeposition mode (RC) is of no less importance. There are reverse (anodic) current pulses in the duty cycle, which make it different from the pulse mode and cause short-term deposit dissolution. Wherein cathodic current pulses alternate with anodic current pulses, as well as with pauses (or without pauses in many works). Pulse-reverse electrodeposition has a complex influence on composition and microstructure of the NiFe alloys (Schultz & Pritzker, 1998; Flynn & Desmulliez, 2010). In the experiments with electrolyte baths similar to ours (sulfate baths with similar additives), a decrease in the Fe content and increased grains vertical growth were described (Wasekar et al., 2016; Williams et al., 1996; Fedosyuk et al., 1991). In our previous work Kotelnikova et al. (2022), we gave a detailed explanation of the mechanism that corresponded to the change in the films composition and grains vertical growth intensity when changing DC and PC modes to RC mode.

In the present work, we analyzed correlation between different modes of electrodeposition (direct current - DC, pulse current - PC and pulse-reverse current - RC) on structural characteristics and magnetic properties of the Ni-rich permalloy films.

2 Experimental

The electrodeposition or electrolyte deposition method was used to obtain alloy NiFe films. The polished steel plates were used as substrates for electrodeposition. The plate width and length were 400 mm, and one side of the plate was isolated by dielectric to deposit film on another side only. The polished steel substrates were chosen for easy films separation from them and following investigations.

The NiFe films were deposited in the complex sulfate electrolyte. The composition of electrolyte presented it Table 1.

Table 1: Chemical composition of electrolyte for preparation of the electrodeposited NiFe films.

Chemical component	**Concentration, g/L**
Main components	
1. $FeSO_4 \cdot 7H_2O$	15
2. $NiSO_4 \cdot 7H_2O$	210
3. $NiCl_2 \cdot 6H_2O$	20
Additional components	
1. H_3BO_3	30
2. $MgSO_4 \cdot 7H_2O$	60
3. $KNaC_4H_4O_6 \cdot 4H_2O$	30
Additives	
1. $C_6H_7O_6$(citric acid)	2
2. $C_7H_5NO_3S$ (saccharin)	2

The electrolyte temperature was kept at 35°C, and the pH was kept at 2.4. The current density was 25 mA/cm^2 for direct and reverse currents. The electrodeposition current parameters are presented in Table 2.

Table 2: The electrodeposition current parameters for NiFe films preparation in direct current mode (DC), pulse mode (PC) and pulse-reverse (RC) modes.

Sample acronym	**Duration of cathodic current (t_C), ms**	**Duration of pause (t_{off}), ms**	**Duration of anodic (reverse) current (t_A), ms**	**Total deposition time, min**	**Effective deposition time, min**
DC	$3.6 \cdot 10^6$	-	-	60	60
PC	100	100	-	120	60
RC	100	75	25	160	60

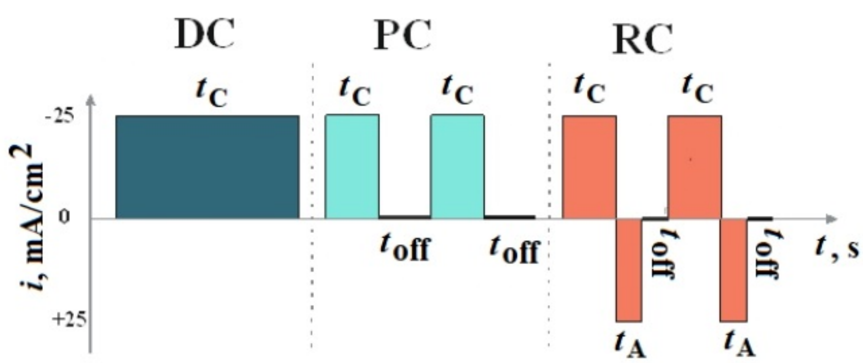

Figure 1: A schematic representation of direct (DC), pulsed (PC) and pulse-reverse (RC) current modes for NiFe films electrodeposition.

The DC sample was obtained in direct current mode for 60 min. The PC sample was deposited in pulse current mode with a cathodic current pulse t_C of 100 ms and an equal pause duration t_{off} for 120 min in total. RC sample was obtained in pulse-reverse current mode with a cathodic current pulse of 100 ms. The anodic (reverse) current pulse t_A was 25 ms and pause was 75 ms. The electrodeposition mode scheme is presented in Figure 1.

The total deposition time and effective deposition time parameters were used to deposit NiFe film with close thicknesses. The total and effective deposition times were equal for the DC sample, as the cathodic current was applied to it continuously. The total deposition time for pulse and pulse-reverse modes was calculated using:

$$t_{TD} = t_{ED} \times \frac{t_C + t_A + t_{OFF}}{t_C - t_A}, \quad (1)$$

where t_{TD} is total deposition time, ms; t_{ED} is effective deposition time, ms; t_C is cathodic current pulse duration, ms; t_{OFF} is pause duration, ms; and t_A is anodic (reverse) current pulse duration, ms.

The chemical composition was investigated by energy-dispersive X-ray spectroscopy on AZtecLive Advanced with Ultim Max 40 (Oxford Instruments, Bognor Regis, UK). The precision of the measurements σ was ± 0.1 at. %. The crystal structure was studied by XRD on the powder diffractometer EMPYREAN (PANalytical, Malvern Instruments, Malvern, UK) using *Cu-K*α radiation in the Bragg–Brentano geometry focusing in the angle range $2\theta = 40 - 100$ °. The coherent scattering regions sizes were estimated using the Williamson–Hall method for all peaks in the fcc solid solution. The precision of the measurements σ was ± 0.01 % for peak intensity, ± $1{\cdot}10^{-4}$ nm for unit cell parameter, and ± 1 nm for coherent scattering region.

The surface microstructure was investigated using the atomic force microscope (AFM) NT-206 (Microtestmachines, Gomel, Belarus). The contact scanning mode was used to obtain AFM images. A silicon tip with a curvature radius of 10 nm and a force constant of 0.6 N/m was used during AFM scanning. Grain sizes were measured using AFM images (20×20 μm) of free films via the Gwyddion software. To recognize the grains, the method of marking grains by the watershed was used.

Thermal analysis was carried out using a differential scanning calorimeter (DSC) 404 F3 Pegasus (NETZSCH, Germany) at a temperature range of 30 – 1500°C in the gaseous atmosphere – argon (Ar). The measurement was carried out at a constant heating rate 10 K/min. The measurement results were processed using the Proteus software supplied with the measuring equipment.

The magnetic parameters were investigated at a temperature range of 4.2 – 900 K using the Liquid Helium Free High Field Measurement System (Vibrating Sample Magnetometer – VSM) (Cryogenic Limited, London, UK). The applied magnetic field was from -3 to +3 T, and the precision of the measurements for specific magnetization σ was ± 0.01 $A{\cdot}m^2{\cdot}kg^{-1}$.

3 Results and discussion

3.1 Structural characteristics

The energy-dispersive X-ray spectroscopy (EDX) was used to investigate the chemical composition of the NiFe films. Figure 2 demonstrates EDX-spectra and elemental mapping for prepared samples. There is an increase in the Fe concentration when changing from DC (36.4 at.%) to pulse current mode (42.1 at.%). The Fe content is increased due to the intensification of the Fe ions diffusion during the pauses.

There is a sharp decrease (from 42.1 to 17.4 at. %) in the Fe content during the transition from pulse (PC sample) to pulse-reverse (RC sample) electrodeposition mode. It is due to the higher Fe than Ni oxidation (and dissolution) rate during anodic pulses as well as Fe hydroxides transfer from the near-sample area into the bulk of the electrolyte during both anodic pulses and pauses, which weakens the anomalous character of the NiFe codeposition. A more detailed description of chemical composition correlations is presented in our previous works (Kotelnikova et al., 2022; Zubar et al., 2021).

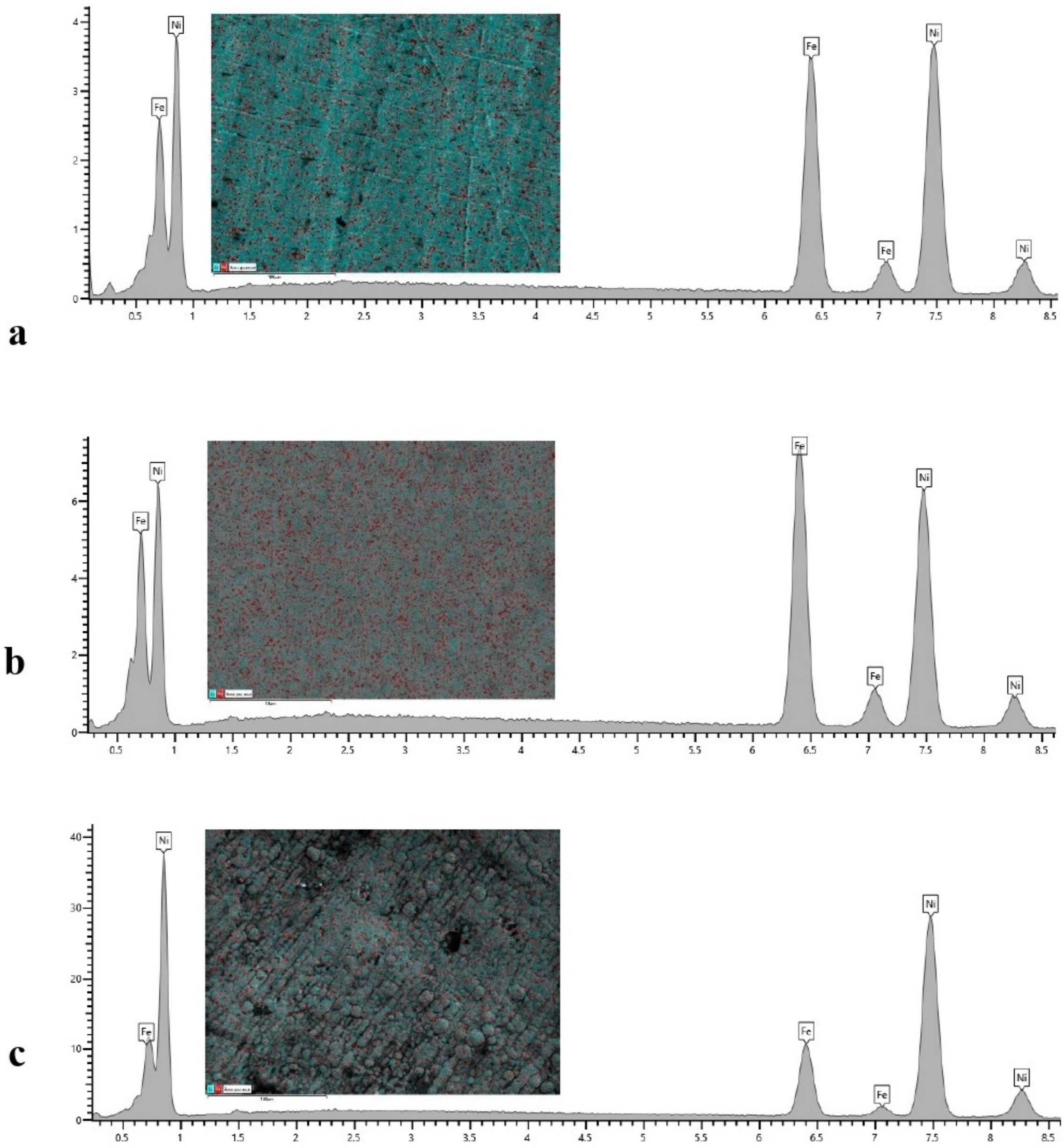

Figure 2: EDX-spectra and elemental mapping (on insert) of the NiFe films prepared in direct current modes: (a) DC; (b) PC and (c) RC.

The X-ray diffraction structural analysis (XRD) patterns are presented in Figure 3. All the peaks correspond to face-centered cubic lattice atomic planes, and no peaks correspond to body-centered atomic planes. It indicates that a Fe solid solution in Ni was formed in all the films samples. Crystal structure parameters obtained from XRD are presented in Table 3.

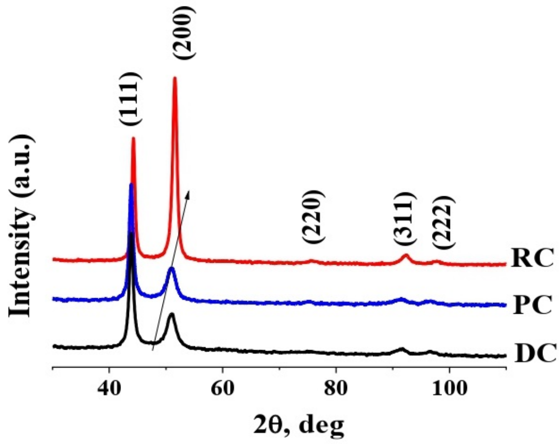

Figure 3: XRD patterns of the NiFe films prepared in direct current modes (DC), pulse mode (PC) and pulse-reverse (RC) modes.

Table 3: Crystal structure parameters of the NiFe films obtained in different electrodeposition modes.

Sample acronym	***a*, nm**	***V*, nm^3**	**I_{200}/I_{111}, %**	**CSR, nm**
DC	0.3570	0.0455	73	˜6
PC	0.3571	0.0455	63	˜7
RC	0.3572	0.0456	211	˜10

The DC and PC samples have very close coherent scattering regions (CSR) sizes and unit cell parameters of ˜6-7 nm. The sample RC has a CSR size of ˜10 nm. There is also a significant increase in the peaks integral intensities ratio $I_{(200)}/I_{(111)}$ with transition from pulse to pulse-reverse mode. It means that film crystals grew in a predominant direction (200) during the pulse-reverse mode.

Figure 4 presents atomic force microscopy (AFM) images of the NiFe films surface. Gwyddion software was used to investigate grain sizes in AFM images. It was impossible to distinguish the grains of the DC and PC films to evaluate their sizes. The DC and PC samples have a smooth surface without distinguishable grains. While DC film has a lot of pores and PC film is almost poreless. Pulse-reversed film surfaces significantly differ from DC and PC films and have observable, mostly fused grains. The reason for such a difference in microstructure is the features of saccharine‘s (brightening additive in the electrolyte) behavior in direct, pulse, and pulse-reverse electrodeposition modes, which were discussed previously (Kotelnikova et al., 2022).

Root mean square (RMS) surface roughness was determined via Gwyddion software from AFM images of the films. DC film has an Rq of 9.6 nm, and PC film has an Rq of 4.1 nm. Surface roughness decreases with the transition from direct to pulse current, which is related to the higher nucleation rate in pulse mode. RC film has Rq value of 27.9 nm. RC film has higher surface roughness than DC and PC films, which is related to promoted grains vertical growth in pulse-reverse mode.

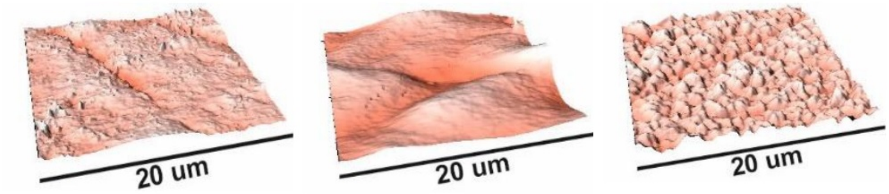

Figure 4: Surface morphology of NiFe films investigated using AFM: (a) DC; (b) PC and (c) RC.

3.2 Phase transitions

Figure 5 demonstrates the results of the differential scanning calorimetry (DSC) investigations of the NiFe films obtained in the different electrodeposition modes. DSC curves include both nonmagnetic second-order phase transition peaks and magnetic second-order phase transition peaks.

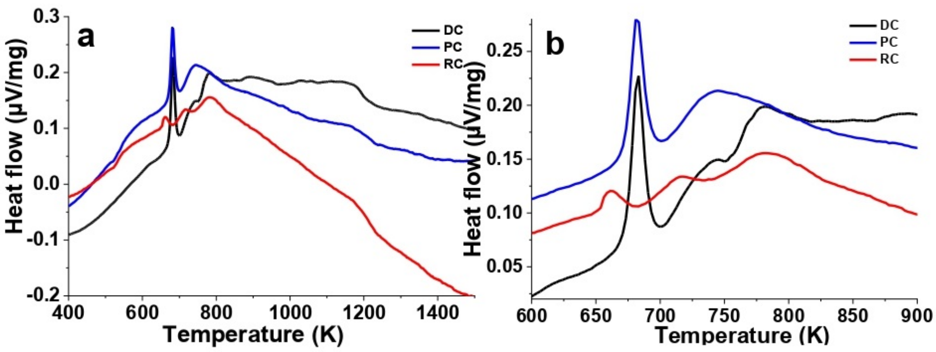

Figure 5: DSC curves of the NiFe films obtained in different electrodeposition modes: in the temperature range 400-1500 K (a) and enlarged DSC curves in the range 600 - 900 K (b).

Nonmagnetic and magnetic phase transition temperatures for bulk NiFe alloys in accordance [53] with compositions similar to NiFe films by us are shown in Table 4.

The temperatures of the nonmagnetic phase transitions (from DSC curves) and proposed phase transitions of the NiFe alloy film are presented in Table 5. It was found that DC film has only two nonmagnetic phase transitions (682 and 744 K) instead of three transitions in the bulk alloy of the same chemical composition (604, 645, and 739 K). The PC sample has only one phase transition instead of two (619 and 787 K). RC film has the same number of phase transitions and very close transition temperatures as the bulk alloy (film – 660 and 718 K, bulk alloy – 678 and 719 K).

Table 4: Phase transitions temperatures of the NiFe bulk alloys (Vernyhora et al., 2012).

Type of phase transition in Ni-Fe system	**Fe concentration, at.%**		
	˜36.4	**˜42.1**	**˜17.4**
$T_{ph}(\alpha - Fe - Ni + FeNi_3 \leftrightarrow FeNi_3)$	604 K	-	-
$T_{ph}(FeNi_3 \leftrightarrow \gamma - Fe - Ni + FeNi_3)$	645 K	-	678 K
$T_{ph}(\gamma - Fe - Ni + FeNi_3 \leftrightarrow \gamma - Fe - Ni)$	739 K	787 K	719 K
$T_{ph}(\alpha - Fe - Ni + FeNi_3 \leftrightarrow \gamma - FeNi + FeNi_3)$	-	619 K	-
$T_{ph}(FeNi_3 \leftrightarrow \gamma - Fe - Ni)$	-	-	-
$T_{ph}(\gamma - Fe - Ni(FM) \leftrightarrow \gamma - Fe - Ni(PM))$	881 K	860 K	819 K

Table 5: Phase transitions temperatures of the NiFe alloy films obtained from DSC curves.

Type of phase transition in Ni-Fe system	**Fe concentration, at.%**		
	˜36.4	˜42.1	˜17.4
	DC	PC	RC
$T_{ph}(a - Fe + FeNi_3 \leftrightarrow g - Fe - Ni)$	-	682 K	-
$T_{ph}(a - Fe + FeNi_3 \leftrightarrow g - Fe - Ni + FeNi_3)$	682 K	-	-
$T_{ph}(g - Fe - Ni + FeNi_3 \leftrightarrow g - Fe - Ni)$	744 K	-	718 K
$T_{ph}(FeNi_3 \leftrightarrow g - Fe - Ni)$	-	-	-
$T_{ph} FeNi_3 \leftrightarrow g - Fe - Ni + FeNi_3)$	-	-	660 K

3.3 Magnetic properties

Figure 6 demonstrates temperature dependences of the magnetic susceptibility (fig. 6a) and concentration dependences of the magnetic phase transition (Curie temperature or T_c) – fig. 6b determined by Faraday technique.

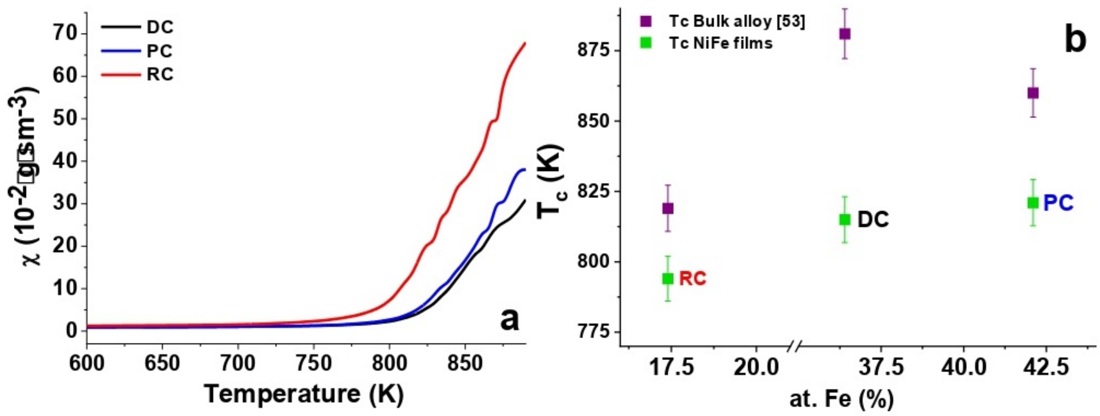

Figure 6: Temperature dependences of the magnetic susceptibility (a) and concentration dependences of the magnetic phase transition (b) determined by Faraday technique.

Results of the NiFe alloy films Curie temperature measurement by Faraday technique are presented also in Table 6. The magnetic transition temperature T_c (Faraday) for DC and PC samples is 815 and 821 K, respectively. RC films has T_c ˜ 794 K.

It was found that all the electrodeposited films have lower Curie temperatures as compared with those in the NiFe phase diagram for bulk NiFe alloys of the same compositions Zubar et al. (2021). That decrease is caused by the transition from bulk to 2D-objects. The Tc values for DC-PC-RC samples correlate well with average Fe content in electrodeposited films.

Figure 7 demonstrates field dependences of the specific magnetization for DC-PC-RC NiFe films. Field dependences of $M(B)$ dependences were measured by VSM in the wide range of magnetic fields (up to 3 T) for perpendicular and parallel orientation to the film surface.

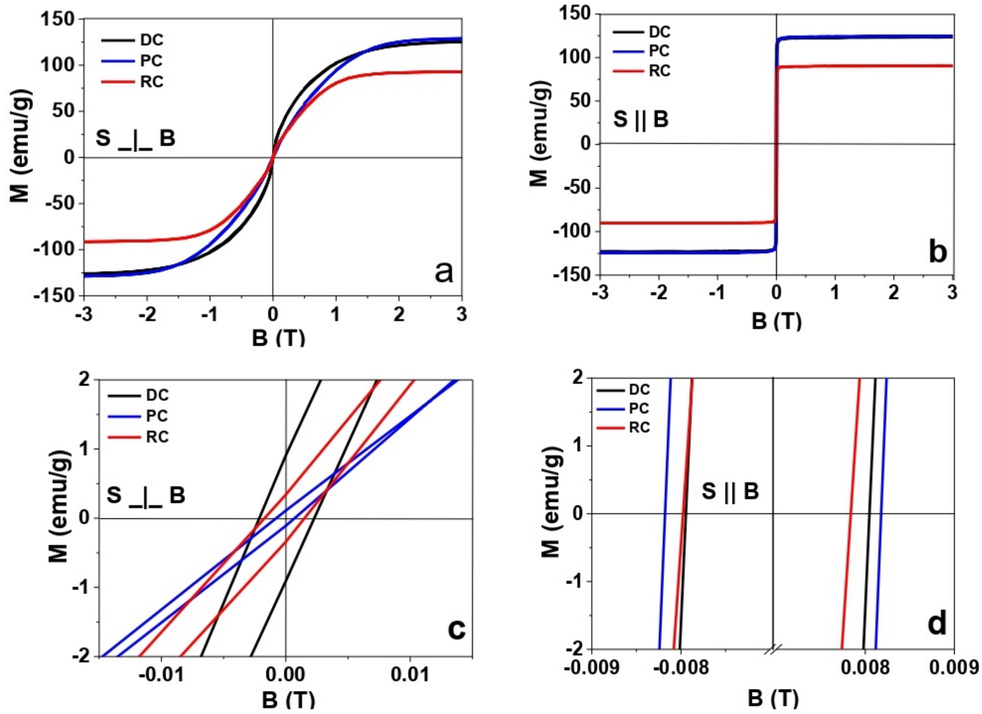

Figure 7: Field dependences of the specific magnetization of the NiFe films obtained in different electrodeposition modes: (a) magnetic field (in the range up to 3 T) oriented perpendicular to the film plane, (b) magnetic field (in the range up to 3 T) oriented parallel to the film plane, (c) enlarged for perpendicular orientation and (d) enlarged for parallel orientation.

Table 6: Main magnetic parameters of the NiFe films obtained in different electrodeposition modes in perpendicular and parallel field orientations: magnetization saturation (M_s); remnant magnetization (M_r); coercivity (H_c); saturation field (H_s) and squareness coefficient (SQR).

Magnetic parameters	Sample acronym		
	DC	PC	RC
	S_|_B		
M_s, emu/g	114.4	121.7	89.8
M_r, emu/g	0.9	0.1	0.4
H_c, Oe	21.5	7.7	17.5
H_s, kOe	19.6	21.7	18.1
SQR (M_r/M_s), $\cdot 10^{-4}$	79	9	38
	S ||B		
M_s, emu/g	121.8	132.6	89.4
M_r, emu/g	108.2	113.1	81.1
H_c, Oe	83.7	87.6	81.9
H_s, kOe	1.4	1.0	1.5
SQR (M_r/M_s), $\cdot 10^{-4}$	8911	8502	9134

The significant magnetic anisotropy of the NiFe films magnetic parameters defined from the $M(B)$ dependences is presented in Table 6. According to the out-of-plane measurements (perpendicular field orientation), the coercivity (H_c) of the sample DC is equal to ~21.5 Oe, whereas the PC film's coercivity is ~7.7 Oe. There is a H_c~17.5 Oe for RC. Saturation field H_s has the following values: DC – 19.6, PC – 21.7 and RC – 18.8 kOe. Saturation magnetization M_s is 114.4, 121.7 and 89.8 emu/g. Remnant magnetization M_r is 0.9, 0.1 and 0.4 emu/g for DC, PC and RC films, respectively. Hysteresis loop squareness M_r/M_s is: DC – 0.0079, PC – 0.0009 and RC – 0.0038.

The easy magnetization axis is located in the plane of all the NiFe films. All the samples have similar values of the $H_c$during the in-plane (parallel orientation) study: DC – 83.7, PC – 87.3 and RC – 81.9 Oe. Saturation field H_s has the following values: DC – 1.4, PC – 1.0 and RC – 1.5 kOe. Saturation magnetization M_s is 121.8, 132.6 and 89.4 emu/g. Remnant magnetization M_r is 108.2, 113.1 and 81.1 emu/g for DC, PC and RC films, respectively. Hysteresis loop squareness M_r/M_s is: DC – 0.8911, PC – 0.8502 and RC25 – 0.9134.

4 Conclusions

A set of NiFe alloy films was electrodeposited in direct, pulse, and pulse-reverse current modes in a single sulfate bath. The samples Fe content varied from 17.4 to 42.1 at. %, depending on deposition modes. It was demonstrated broad perspectives for chemical control (Fe/Ni ratio) of the electrodeposited Ni-rich permalloy films from one electrolyte. This is technologically convenient. All the samples showed characteristic peaks of fcc lattice atomic planes during XRD investigations. It indicates that all samples are single-phase and Fe solid solution in Ni was formed in all the film samples.

Pulse-reverse (RC) film surface are rough and have observable mostly fused grains, which significantly differs from DC and PC film surfaces, which are smooth and have no distinguishable grains. The R_q values of RC film is around 27.9 nm, while DC and PC films have R_q values of 9.6 nm and 4.1 nm, respectively.

According to the DSC investigations, all the electrodeposited films have different numbers of nonmagnetic phase transitions and transition temperatures from their bulk analogs in the NiFe phase diagram in (Vernyhora *et al.*, 2012).

The synthesized NiFe films have a significant magnetic anisotropy. The coercive force H_c of the NiFe films during the sample in plane investigations is $\sim$ 2–12 times greater than during sample out of plane investigations. Remnant magnetization M_r of the NiFe films during the sample in plane investigations is $\sim$ 40–1000 times greater than during sample out of plane investigations.

Obtained results open broad perspectives for Ni-rich permalloy films preparation with variable Fe content and different microstructure for practical applications in the field of magnetic sensors and shields for electromagnetic protection.

Acknowledgement.
Investigations were supported by the Science Committee of the Ministry of Science and Higher Education of the Republic of Kazakhstan (No. AP19680155).

References

Almeida, T.P., Lequeux, S., Palomino, A., Sousa, R.C., Fruchart, O., Prejbeanu, I.-L., ..., & Cooper, D. (2022). Quantitative visualization of thermally enhanced perpendicular shape anisotropy STT-MRAM nanopillars. *Nano Letters, 22*, 4000-4005. https://doi.org/10.1021/acs.nanolett.2c00597

Blythe, H.J., Fedosyuk, V.M., & Kasyutich, O.I. (1996). Chemically deposited CuCo granular films: an alternative route to GMR. *Materials Letters, 26*, 69-72. https://doi.org/https://doi.org/10.1016/0167-577X(95)00207-3

Deligianni, H. (2006). Electrodeposition and microelectronics. *The Electrochemical Society Interface*, 15, 33. https://doi.org/10.1149/2.F09061IF

English, A.T., Chin, G.Y. (1967). Metallurgy and magnetic properties control in permalloy. *Journal of Applied Physics*, 38, 1183-1187. https://doi.org/10.1063/1.1709532

Fedkin, V., Fedosyk, V., Kotelnikova, A., Kanafyev, O., Panasiuk, M., Usovich, T., ... , & Trukhanov, A. (2023). Features of pulse-reverse modes for Ni–Fe nanogranular films electrodeposition: Correlation of structural parameters and MI effect. *Ceramics International*, 49, 28089-28097. https://doi.org/https://doi.org/10.1016/j.ceramint.2023.06.058

Fedosyuk, V.M., Kasyutich, O.I., & Kozich, N.N. (1991). Electrodeposition and study of multilayered Co/Cu structures. *Journal of Materials Chemistry*, 1, 795-797. https://doi.org/10.1039/JM9910100795

Flynn, D., Desmulliez, M.P.Y. (2010). Influence of pulse reverse plating on the properties of Ni-Fe thin films. *IEEE Transactions on Magnetics*, 46, 979-985. https://doi.org/10.1109/TMAG.2009.2036723

Giurlani, W., Zangari, G., Gambinossi, F., Passaponti, M., Salvietti, E., Di Benedetto, F.,..., & Innocenti, M. (2018). Electroplating for decorative applications: Recent trends in research and development. *Coatings,* 8, 260. https://doi.org/10.3390/coatings8080260

Graf, W., Vance, E.F. (1988). Shielding effectiveness and electromagnetic protection. IEEE Transactions on Electromagnetic Compatibility, 30, 289-293. https://doi.org/10.1109/15.3307

Grimmett, D.L., Schwartz, M., & Nobe, K. (1993). A Comparison of DC and pulsed Fe-Ni alloy deposits. *Journal of The Electrochemical Society*, 140, 973–978. https://doi.org/10.1149/1.2056238

Horkans, J. (1981). Effect of plating parameters on electrodeposited NiFe. *Journal of The Electrochemical Society,* 128, 45-49. https://doi.org/10.1149/1.2127385

Hika, K., Panina, L.V., & Mohri, K. (1996). Magneto-impedance in sandwich film for magnetic sensor heads. *IEEE Transactions on Magnetics*, 32, 4594–4596. https://doi.org/10.1109/20.539090

Inguanta, R., Piazza, S., & Sunseri, C. (2008). Influence of electrodeposition techniques on Ni nanostructures. *Electrochimica Acta*, 53, 5766-5773. https://doi.org/10.1016/j.electacta.2008.03.045

Jeong, W.-C., Lee, B.-I., & Joo, S.-K. (1998). A new multilayered structure for multilevel magnetoresistive random access memory (MRAM) cell. *IEEE Transactions on Magnetics*, 34, 1069-1071. https://doi.org/10.1109/20.706359

Kanafyev, O.D., Trukhanov, A.V., Zubar, T.I., Grabchikov, S.S., Panasiuk, M.I., Kotelnikova, A.N., ...,& Fedosyuk, V.M. (2022). Influence of cylindrical shield dimensions on shielding effectiveness. *Devices and Methods of Measurements*, 13, 112-116. https://doi.org/10.21122/2220-9506-2022-13-2-112-116

Kockar, H., Alper, M., & Topcu, H. (2004). Effect of potantiostatic waveforms on properties of electrodeposited NiFe alloy films. *The European Physical Journal B*, 42, 497-501. https://doi.org/10.1140/epjb/e2005-00008-8

Kotelnikova, A., Zubar, T., Vershinina, T., Panasyuk, M., Kanafyev, O., Fedkin, V.,...,& Trukhanov, A. (2022). The influence of saccharin adsorption on NiFe alloy film growth mechanisms during electrodeposition. *RSC Advances*, 12, 35722-35729. https://doi.org/10.1039/d2ra07118e

Lee, W.Y., Toney, M.F., & Mauri, D. (2000). High magnetoresistance in sputtered permalloy thin films through growth on seed layers of (Ni0.81Fe0.19)1-xCrx. *IEEE Transactions on Magnetics,* 36, 381-385. https://doi.org/10.1109/20.822551

Lelevic, A., Walsh, F.C. (2019). Electrodeposition of NiP alloy coatings: a review. *Surface and Coatings Technology*, 369, 198-220. https://doi.org/10.1016/j.surfcoat.2019.03.055

Lisenkov, A., Zheludkevich, M.L., & Ferreira, M.G.S. (2010). Active protective Al–Ce alloy coating electrodeposited from ionic liquid. *Electrochemistry Communications*, 12, 729-732. https://doi.org/10.1016/j.elecom.2010.03.018

Llavona, Á., Pérez, L., Sánchez, M.C., & De Manuel, V. (2013). Enhancement of anomalous codeposition in the synthesis of Fe-Ni alloys in nanopores. *Electrochimica Acta,* 106, 392-397. https://doi.org/10.1016/j.electacta.2013.05.116

Maniam, K.K., Paul, S. (2021). Corrosion performance of electrodeposited zinc and zinc-alloy coatings in marine environment. *Corrosion and Materials Degradation*, 2, 163-189. https://doi.org/10.3390/cmd2020010

Mazraati, H., Chung, S., Houshang, A., Dvornik, M., Piazza, L., Qejvanaj, F.,..., & Åkerman, J. (2016). Low operational current spin Hall nano-oscillators based on NiFe/W bilayers. *Applied Physics Letters,* 109, 1-5. https://doi.org/10.1063/1.4971828

Ma, T.Y., Wan, C.H., Wang, X., Yang, W.L., Guo, C.Y., Fang, C., ... ,& Han, X.F. (2020). Evidence of magnetization switching by anomalous spin Hall torque in NiFe. *Physical Review B*, 101, 1-6. https://doi.org/10.1103/PhysRevB.101.134417

Nasirpouri, F. (2017). *Electrodeposition of nanostructured materials.* Springer. https://doi.org/10.1007/978-3-319-44920-3

Oriňáková, R., Turoňová, A., Kladeková, D., Gálová, M., & Smith, R.M. (2006). Recent developments in the electrodeposition of nickel and some nickel-based alloys. *Journal of Applied Electrochemistry,* 36, 957-972. https://doi.org/10.1007/s10800-006-9162-7

Papailiou, M., Dimitrova, S., Babayev, E.S., & Mavromichalaki, H. (2010). Analysis of changes of cardiological parameters at middle latitude region in relation to geomagnetic disturbances and cosmic ray variations. *AIP Conference Proceedings*, 1203, 748. https://doi.org/10.1063/1.3322548

Pasa, A.A., Schwarzacher, W. (1999). Electrodeposition of thin films and multilayers on silicon. *Physica Status Solidi (A) Applications and Materials Science*, 173, 73–84. https://doi.org/10.1002/(SICI)1521-396X(199905)173:1<73::AID-PSSA73>3.0.CO;2-8

Park, J.H., Lee, J.W., Choi, H.J., Jang, W.G., Kim, T.S., Suh, D.S., ... , & Suh, S.J. (2019). Electromagnetic interference shielding effectiveness of sputtered NiFe/Cu multi-layer thin film at high frequencies. *Thin Solid Films*, 677, 130-136. https://doi.org/10.1016/j.tsf.2019.03.015

Rizal, C., Niraula, B.B. (2015). Ferromagnetic alloys: magnetoresistance, microstructure, magnetism, and beyond (review). *Journal of Nano- and Electronic Physics*, 7, 04068.

Rotkovich, A.A., Tishkevich, D.I., Bondaruk, A.A., German, S.A., Razanau, I.U., Zubar, T.I., ... , & Trukhanov, A.V. (2023). Epoxy-W composite materials: microstructure, structure, and radiation efficiency. *Advanced Physical Research*, 5, 133-145.

Stine, K.J. (2019). Biosensor applications of electrodeposited nanostructures. *Applied Sciences*, 9, 797. https://doi.org/10.3390/app9040797

Sobha Jayakrishnan, D. (2012). Electrodeposition: the versatile technique for nanomaterials, Woodhead Publishing Limited, 2012. https://doi.org/10.1533/9780857095800.1.86

Suzdaltsev, A. (2022). Silicon electrodeposition for microelectronics and distributed energy: A mini-review. *Electrochem*, 3, 760-768. https://doi.org/10.3390/electrochem3040050

Salem, M.S., Sergelius, P., Zierold, R., Montero Moreno, J.M., Görlitz, D., & Nielsch, K. (2012). Magnetic characterization of nickel-rich NiFe nanowires grown by pulsed electrodeposition. *Journal of Materials Chemistry*, 22, 8549-8557. https://doi.org/10.1039/c2jm16339j

Schultz, H., Pritzker, M. (1998). Modeling the galvanostatic pulse and pulse reverse plating of nickel-iron alloys on a rotating disk electrode. *Journal of The Electrochemical Society,* 145, 2033-2042. https://doi.org/10.1149/1.1838594

Seet, H.L., Li, X.P., Lee, K.S., & Chia, H.Y. (2007). Nanocrystalline grain size control for Ni80Fe20/Cu micro-composite wires by different electrodeposition methods. *Journal of Materials Processing Technology*, 192-193, 225–228. https://doi.org/10.1016/j.jmatprotec.2007.04.019

Sousa, R.C., Chavent, A., Iurchuk, V., Vila, L., Ebels, U., Dieny, B., ... & Prejbeanu, I. L. (2020, June). Magnetic random access memories (MRAM) beyond information storage. In 2020 *IEEE Symposium on VLSI Technology* (pp. 1-2). IEEE.. https://doi.org/10.1109/VLSITechnology18217.2020.9265053

Torabinejad, V., Aliofkhazraei, M., Assareh, S., Allahyarzadeh, M.H., & Rouhaghdam, A.S. (2017). Electrodeposition of Ni-Fe alloys, composites, and nano coatings–A review. *Journal of Alloys and Compounds*, 691, 841-859. https://doi.org/10.1016/j.jallcom.2016.08.329

Vahdati Yekta, P., Ghasemi, A., & Sharifi, E.M. (2018). Magnetic and mechanical properties of cold-rolled permalloy. *Journal of Magnetism and Magnetic Materials*, 468, 155-163. https://doi.org/10.1016/j.jmmm.2018.07.088

Vernyhora, I., Tatarenko, V., & Bokoch, S. (2012). Thermodynamics of f.c.c.-Ni–Fe alloys in a static applied magnetic field. *ISRN Thermodynamics*, 2012. https://doi.org/10.5402/2012/917836

Vieux-Rochaz, L., Cuchet, R., & Vaudaine, M.H. (2000). A new GMR sensor based on NiFe/Ag multilayers. *Sensors and Actuators A: Physical*, 81, 53-56. https://doi.org/10.1016/S0924-4247(99)00115-6

Vinnik, D.A., Starikov, A.Y., Zhivulin, V.E., Astapovich, K.A., Turchenko, V.A., Zubar, T.Y.I., ... & Trukhanov, A.V. (2021). Changes in the structure, magnetization, and resistivity of BaFe12–x Ti x O19. *ACS Applied Electronic Materials, 3*(4), 1583-1593. https://doi.org/10.1021/acsaelm.0c01081

Warcholinski, B., Gilewicz, A., Kuznetsova, T.A., Zubar, T.I., Chizhik, S.A., Abetkovskaia, S.O., & Lapitskaya, V.A. (2017). Mechanical properties of Mo(C)N coatings deposited using cathodic arc evaporation. *Surface and Coatings Technology*, 319, 117-128. https://doi.org/https://doi.org/10.1016/j.surfcoat.2017.04.005

Wasekar, N.P., Haridoss, P., Seshadri, S.K., & Sundararajan, G. (2016). Influence of mode of electrodeposition, current density and saccharin on the microstructure and hardness of electrodeposited nanocrystalline nickel coatings. *Surface and Coatings Technology,* 291, 130-140. https://doi.org/10.1016/j.surfcoat.2016.02.024

Williams, J.M., Blythe, H.J., & Fedosyuk, V.M. (1996). An investigation of electrodeposited granular CuFe alloyed films. *Journal of Magnetism and Magnetic Materials,* 155, 355-357. https://doi.org/10.1016/0304-8853(95)00693-1

Zangari, G. (2015). Electrodeposition of alloys and compounds in the era of microelectronics and energy conversion technology. *Coatings,* 5, 195-218. https://doi.org/10.3390/coatings5020195

Zhang, B., Fenineche, N.E., Zhu, L., Liao, H., & Coddet, C. (2012). Studies of magnetic properties of permalloy (Fe30 % Ni) prepared by SLM technology. *Journal of Magnetism and Magnetic Materials*, 324, 495-500. https://doi.org/10.1016/j.jmmm.2011.08.030

Zhu, L.J., Ralph, D.C., & Buhrman, R.A. (2018). Irrelevance of magnetic proximity effect to spin-orbit torques in heavy-metal/ferromagnet bilayers. *Physical Review B*, 98, 1-5. https://doi.org/10.1103/PhysRevB.98.134406

Zubar, T.I., Chizhik, S.A. (2019). Studying nanotribological properties of functional materials via Atomic Force Microscopy. *Journal of Friction and Wear*, 40, 201-206. https://doi.org/10.3103/S1068366619030140

Zubar, T.I., Fedosyuk, V.M., Trukhanov, A.V., Kovaleva, N.N., Astapovich, K.A., Vinnik, D.A., ..., & Trukhanov, S.V. (2019). Control of growth mechanism of electrodeposited nanocrystalline NiFe films. *Journal of The Electrochemical Society*, 166, D173-D180. https://doi.org/10.1149/2.1001904jes

Zubar, T.I., Usovich, T.I., Tishkevich, D.I., Kanafyev, O.D., Fedkin, V.A., Kotelnikova, A.N.,...,& Trukhanov, A.V. (2022). Features of galvanostatic electrodeposition of NiFe films with composition gradient: influence of substrate characteristics. *Nanomaterials*, 12, 2926. https://doi.org/10.3390/nano12172926

Zubar, T., Fedosyuk, V., Tishkevich, D., Kanafyev, O., Astapovich, K., Kozlovskiy, A.,..., & Trukhanov, A. (2020). The effect of heat treatment on the microstructure and mechanical properties of 2d nanostructured au/nife system. *Nanomaterials*, 10, 1-14. https://doi.org/10.3390/nano10061077

Zubar, T., Grabchikov, S., Kotelnikova, A., Kaniukov, E., Kutuzau, M., Leistner, K.,..., & Trukhanov, A. (2021). Efficiency of magnetostatic protection using nanostructured permalloy shielding coatings depending on their microstructure. *Nanomaterials,* 11, 1-13. https://doi.org/10.3390/nano11030634